

Tailored and universal parallel transmit broadband pulses for homogeneous 3D excitation of the human heart at 7T

Christoph Stefan Aigner¹  | Sebastian Dietrich-Conzelmann¹  | Max Lutz¹  |
Felix Krüger¹  | Sebastian Schmitter^{1,2,3} 

¹Physikalisch-Technische Bundesanstalt (PTB), Braunschweig and Berlin, Germany

²University of Minnesota, Center for Magnetic Resonance Research, Minneapolis, Minnesota USA

³Medical Physics in Radiology, German Cancer Research Center (DKFZ), Heidelberg, Germany

Correspondence

Christoph Stefan Aigner,
Physikalisch-Technische Bundesanstalt (PTB), Braunschweig and Berlin Germany.
Email: christoph.aigner@ptb.de

Funding information

German Research Foundation,
Grant/Award Numbers: GRK2260, SCHM 2677/2-1, SCHM 2677/4-1; BIOQIC

Abstract

Purpose: To research and evaluate the performance of broadband tailored kT-point pulses (TP) and universal pulses (UP) for homogeneous excitation of the human heart at 7T.

Methods: Relative 3D B_1^+ -maps of the thorax were acquired from 29 healthy volunteers. TP and UP were designed using the small-tip-angle approximation for a different composition of up to seven resonance frequencies. TP were computed for each of the 29 B_1^+ -maps, and UPs were calculated using 22 B_1^+ -maps and tested in seven testcases. The performance of the pulses was analyzed using the coefficient of variation (CV) in the 3D heart volumes. The 3D gradient-echo (GRE) scans were acquired for the seven testcases to qualitatively validate the B_1^+ -predictions.

Results: Single- and double-frequency optimized pulses achieved homogeneity in flip angle (FA) for the frequencies they were optimized for, while the broadband pulses achieved uniformity in FA across a 1300 Hz frequency range.

Conclusion: Broadband TP and UP can be used for homogeneous excitation of the heart volume across a 1300 Hz frequency range, including the water and the main six fat peaks, or with longer pulse durations and higher FAs for a smaller transmit bandwidth. Moreover, despite large inter-volunteer variations, broadband UP can be used for calibration-free 3D heart FA homogenization in time-critical situations.

KEYWORDS

7 Tesla, body MRI, broadband, parallel transmission, universal pulse

Parts of this work have been presented at the 2022 Annual Meeting of the International Society for Magnetic Resonance in Medicine.

This is an open access article under the terms of the [Creative Commons Attribution](https://creativecommons.org/licenses/by/4.0/) License, which permits use, distribution and reproduction in any medium, provided the original work is properly cited.

© 2024 Physikalisch-Technische Bundesanstalt. *Magnetic Resonance in Medicine* published by Wiley Periodicals LLC on behalf of International Society for Magnetic Resonance in Medicine.

1 | INTRODUCTION

Ultra-high field (UHF) MRI has shown great promise in enabling high-resolution imaging and accurate quantification of human tissue.^{1,2} One particularly compelling application of UHF MRI is its potential to detect and characterize even small fat infiltration within the myocardium at 7T, which can serve as an early indicator of heart disease and a predictor of mortality in patients with heart failure.^{3–5} Despite these promising advancements, UHF MRI, particularly in the context of cardiac fat/water imaging, also presents several challenges that require careful consideration and thoughtful approaches for successful implementation.^{1,2}

One such challenge is the inherent inhomogeneity of the transmit field (B_1^+) at UHF, resulting in spatially varying flip angle (FA) and potential FA dropouts. This variability in FAs across the target region affects image contrast and, therefore, compromises diagnostic accuracy. Although various approaches have been developed to address the inhomogeneous transmit field,^{2,6–8} the application of UHF MRI to the human body, which is usually larger in size than the human brain, requires specialized methodologies to tackle this issue effectively. Furthermore, multiple sources of motion, including respiration, cardiac activity, and blood flow, exacerbate the technical challenges encountered in UHF MRI when targeting areas within the human body, such as the heart or liver.^{9–14}

A range of innovative solutions has been proposed to address these challenges, encompassing the integration of multi-transmit RF coils and parallel transmission (pTx) techniques^{15–21} using volunteer-specific B_1^+ information alongside motion-robust non-Cartesian acquisition schemes and advanced reconstruction approaches.^{11,22,23} Dynamic pTx employs, in contrast to static pTx, temporally changing RF and gradient waveforms. Such pulses are known to be susceptible to variations in the main magnetic field (ΔB_0).⁸ While dynamic pTx pulses can be designed with a short pulse duration to be less sensitive to ΔB_0 variations,^{12,24} they can also be optimized to compensate for local ΔB_0 deviations by including measured ΔB_0 information, thereby mitigating their impact on image quality and diagnostic accuracy.^{8,21,25,26}

A fundamental problem with designing such tailored pulses in the human body is the adjustment time of 10–15 min required to acquire volunteer specific $B_1^+/\Delta B_0$ information, design, and apply the tailored pTx pulses. This issue has been successfully addressed using universal pulses (UP) in the human brain^{27–29} and the human body targeting the heart.^{30,31} However, such UPs cannot be applied straightforwardly for fat/water separation

techniques at 7T,⁵ since the resonant frequencies of fat span a range of approximately 1300 Hz at 7T. Since both UP and TP are designed to excite a single frequency, typically water, they might result in reduced excitation fidelity for other frequencies, such as those within the fat spectrum. This limitation hinders, for example, successful fat/water separation using a Dixon approach,^{32–34} a CSI technique that relies on the in-phase/out-of-phase cycling of fat and water signals.

Broadband pTx has been demonstrated to be effective for various applications, including slab-selective spokes pulses³⁵ or non-selective excitation and refocusing pulses using Gradient Ascent Pulse Engineering (GRAPE).^{36,37} In contrast to designing the pulse for a single resonance frequency, these techniques utilize pulses designed at multiple resonance frequencies to compensate for ΔB_0 field variations in specific target regions in the human brain, such as the sinuses and the left cerebellum.³⁷

This work builds upon these previous findings by introducing two novel contributions: First, we demonstrate the feasibility of UHF broadband pTx pulses for simultaneous fat/water excitation in the human body, enabling fat/water separation techniques like Dixon.^{32–34} Second, we introduce broadband TP and UP that eliminate the need for measured ΔB_0 information, as previously required in dynamic pTx approaches.^{8,19,21,26} Experimental data at 7T validate the B_1^+ predictions and indicate the successful excitation of fat and water in the human heart at 7T.

2 | METHODS

2.1 | Volunteer information and MR scanner hardware

MRI data was acquired in adherence to an approved Institutional Review Board (IRB) protocol with a 7T MR system (Siemens Magnetom, Germany) using a commercial 32-element body coil array (MRI.TOOLS, Germany) operating in 8TX/32RX (transmit/receive) mode. Volunteers were divided into library (14 Male/8 Female, 21–66 years and 19–35 kg/m²) and testcases (5 males/2 females, 22–40 years and 20–25 kg/m²). The posterior coil half was centered on the volunteer's heart in head-foot direction, whereas the anterior coil half was placed based on anatomic landmarks and feedback from the volunteer with a 2 cm gap to the volunteer's chin. The safety limits were meticulously executed following established protocols and consistent with previous studies conducted in this field.^{5,11,12,30,31,38}

2.2 | Adjustments and calibration scans

For each volunteer, 3D relative B_1^+ -maps of the thorax were acquired using a radial phase-encoding (RPE) trajectory during shallow breathing conditions throughout the scanning process (TE/TR = 2.02 ms/5 ms, voxel-size = $4 \times 4 \times 4 \text{ mm}^3$ and FOV = $250 \times 312 \times 312 \text{ mm}^3$, TA = 3 min 25 s).¹¹ The acquired raw files were exported to a workstation (12 cores with 2.1 GHz, 128 GB RAM) and reconstructed in approximately 1 min with a non-respiratory resolved reconstruction with an isotropic spatial resolution of 4 mm. The resulting 3D channel-wise B_1^+ -maps were subsequently employed in designing and evaluating TPs and UPs for this study.

2.3 | Pulse design and evaluation

The pulse design was implemented in MATLAB using the small-tip-angle approximation with an interleaved greedy and local optimization^{21,26} to achieve a target FA of 10° in the heart volume. The heart region was manually selected covering the entire heart on a slice-by-slice basis based on the sum of B_1^+ magnitudes over the TX channels for every volunteer. The kT-points pulses were optimized using the integrated RF power and the root mean squared error of the FA and were implemented using a power limit per TX channel. Each pulse consists of four 0.15 ms long square RF pulses and four 0.09 ms long 3D gradient blips, leading to a total pulse duration of 0.96 ms. The starting phases of the pulse design and the regularization parameters (4.64/107.97 for TP/UP) have been adopted from L-curve analysis with 200 random initial phase combinations from our previous work.³¹ The source code, the used parameters, and the 3D relative B_1^+ datasets can be found at: https://github.com/chaigner/FRobUP_body.

In this work, three distinct types of TP/UP were designed and evaluated relative to the Larmor frequency of water protons at 7T of 298 MHz: (i) TP_S/UP_S optimized for a single frequency at 0 Hz, (ii) TP_D/UP_D optimized for two frequency peaks (0 and 1010 Hz), and (iii) broadband TP_{BB}/UP_{BB} optimized for seven frequency peaks ranging from -178 to 1129 Hz. It is important to note that only the specified frequencies are explicitly considered during the optimization process. All other frequencies are treated as a “don’t care” region, allowing for greater flexibility and control over the pulse design. The following symbols will be used to differentiate between the different frequencies in this work: f_S (single-frequency; 0 Hz), f_D (double-frequency; 1010 and 0 Hz), and f_{BB} (broadband; 1129, 1010, 772, 576, 115, 0, and -178 Hz).

TP were computed individually for each B_1^+ -dataset while UP were computed using all 22 B_1^+ -maps.³¹ Both

pulse types were designed to generate a homogenous FA distribution across the heart volume for different frequencies.

ΔB_0 offsets were added to all spatial points in the optimization to incorporate up to seven frequencies, including water and six fat peaks.³⁹ The measured B_1^+ and synthetic uniform ΔB_0 maps at these frequencies were stacked and fed into the pulse design algorithm, following the same procedure as for the UP design. For instance, in the case of UP_{BB} , the design library contains 22 B_1^+ and 154 ΔB_0 datasets, resulting from 22 volunteers and seven ΔB_0 offsets.

The mean computation time required for generating a TP ranged between 20 s (TP_S) and 99 s (TP_{BB}), while the computation time for the UP ranged between 2 min (UP_S) and 10 min (UP_{BB}). The optimization time for individual volunteers varied from 14 to 32 s for TP_S and 49 to 153 s for TP_{BB} . This results in approximately 10 to 15 min of adjustment time for the whole pipeline to perform subject-tailored pTx of the human heart. This includes data acquisition (3 min 25 s), offline non-Cartesian reconstruction (1 min), manual 3D region of interest (ROI) placement (3 min), pulse design (1–2 min), and variable extra time for checking the results.

The performance of the pulses was assessed using the FA coefficient of variation (CV) within the 3D heart volumes and the integrated RF power. The RF amplitudes were scaled to achieve an average FA of 10 degrees at a ΔB_0 offset of 0 Hz.

2.4 | Simulation studies

A simulation study examined the impact of pulse duration on TP and UP performance. Each pulse was simulated 19 times, using linearly scaled pulse durations from 0.384 ms to 3.840 ms, with RF adjustments to maintain the FA. FA simulations were conducted for all testcases with 201 ΔB_0 offsets (-2500 to 1500 Hz). It is important to note that re-optimizing the pulse for a longer or shorter pulse duration could necessitate a different number of kT points, potentially impacting pulse performance.

The mean and SD of the FA in all heart volumes was calculated for each pulse type, pulse duration, and ΔB_0 offset. Based on the mean FA values for the different ΔB_0 offsets, the transmit bandwidth was determined where the pulses achieved a mean FA exceeding 9° , corresponding to a maximal deviation of 10% from the target FA of 10° .

2.5 | Statistical analysis

To assess statistical significance, we employed the Mann–Whitney *U*-test, assuming independent samples

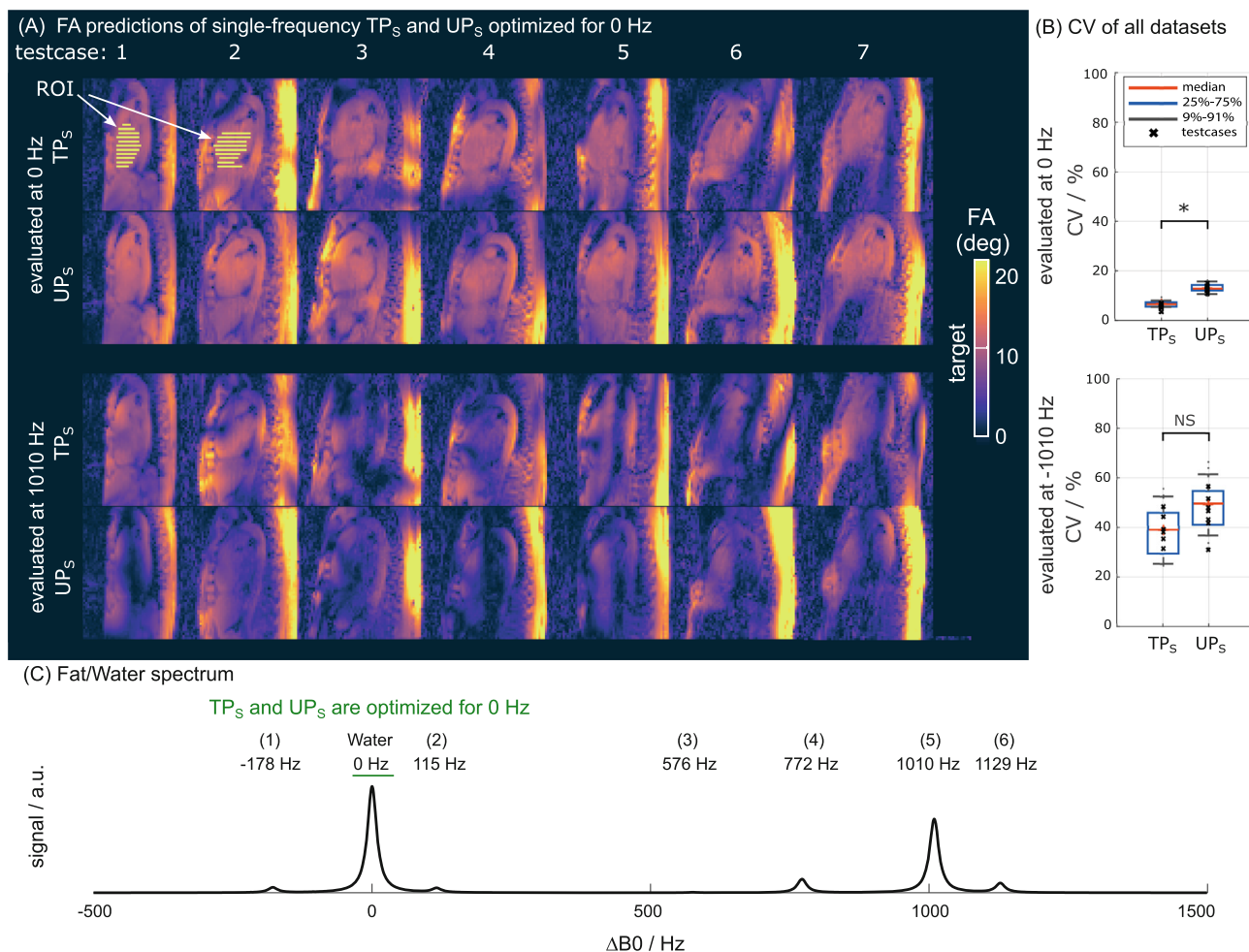


FIGURE 1 FA predictions of tailored and universal pTx pulses (TP_S/UP_S) optimized for water ($f_s = 0$ Hz) and evaluated at 0 Hz (water) and 1010 Hz (main fat peak at 7T). (A) Sagittal views of the 3D volume illustrate the FA homogeneity at the water frequency and the spatial variations and dropouts observed at the fat frequency. (B) Quantitative assessment of predicted FA homogeneity across the entire target volumes of all datasets evaluated at 0 Hz and 1010 Hz. Statistically significant outcomes are denoted by a star (*), while non-statistically significant results are indicated as “NS”. (C) Model fat and water spectrum indicating which frequencies have been optimized in the pulse design. Peak numbering (1), (2), etc. is taken from Hamilton et al.⁴⁰

from two groups with continuous distributions and equal medians. The significance level was set to 5%.

2.6 | Experimental validation of optimized pulses

The 3D RPE gradient echo (GRE) scans were acquired in three phantoms (rapeseed oil, CuSu doped water, and polyvinylpyrrolidone [PVP]) and five testcases to validate the efficacy of TP_S/TP_{BB} using the following parameters: $TE/TR = 1.58$ ms/2.75 ms, $FOV = 256 \times 256 \times 256$ mm³, voxel-size = $4 \times 4 \times 4$ mm, $TA = 135$ s. While the water/oil phantoms were used to demonstrate the performance of TP_{BB} , a set of 10 PVP phantom scans were acquired by manually setting the resonance frequency from -2000 to 1000 Hz (w.r.t. the vendor supplied frequency scout)

to test the broadband properties of TP_S , TP_D , and TP_{BB} (see Figure S1). Additionally, in two additional testcases, higher resolution 3D RPE GRE scans were acquired with TP_S , TP_{BB} , and UP_{BB} using the following parameters: $TE/TR = 1.58$ ms/3.38 ms, $FOV = 250 \times 250 \times 250$ mm³, voxel-size = $2 \times 2 \times 2$ mm, $TA = 221$ s. Note that all RF pulses were implemented with the same peak RF voltage of 104 V to stay below the power-per-channel limits of our specific absorption rate (SAR) supervision using the minimal TE/TR combination for each sequence, resulting in potentially different FAs for the different pulses.

3 | RESULTS

Figure 1 presents the FA predictions of single-frequency optimized TP_S/UP_S with a fixed pulse duration of 0.96 ms

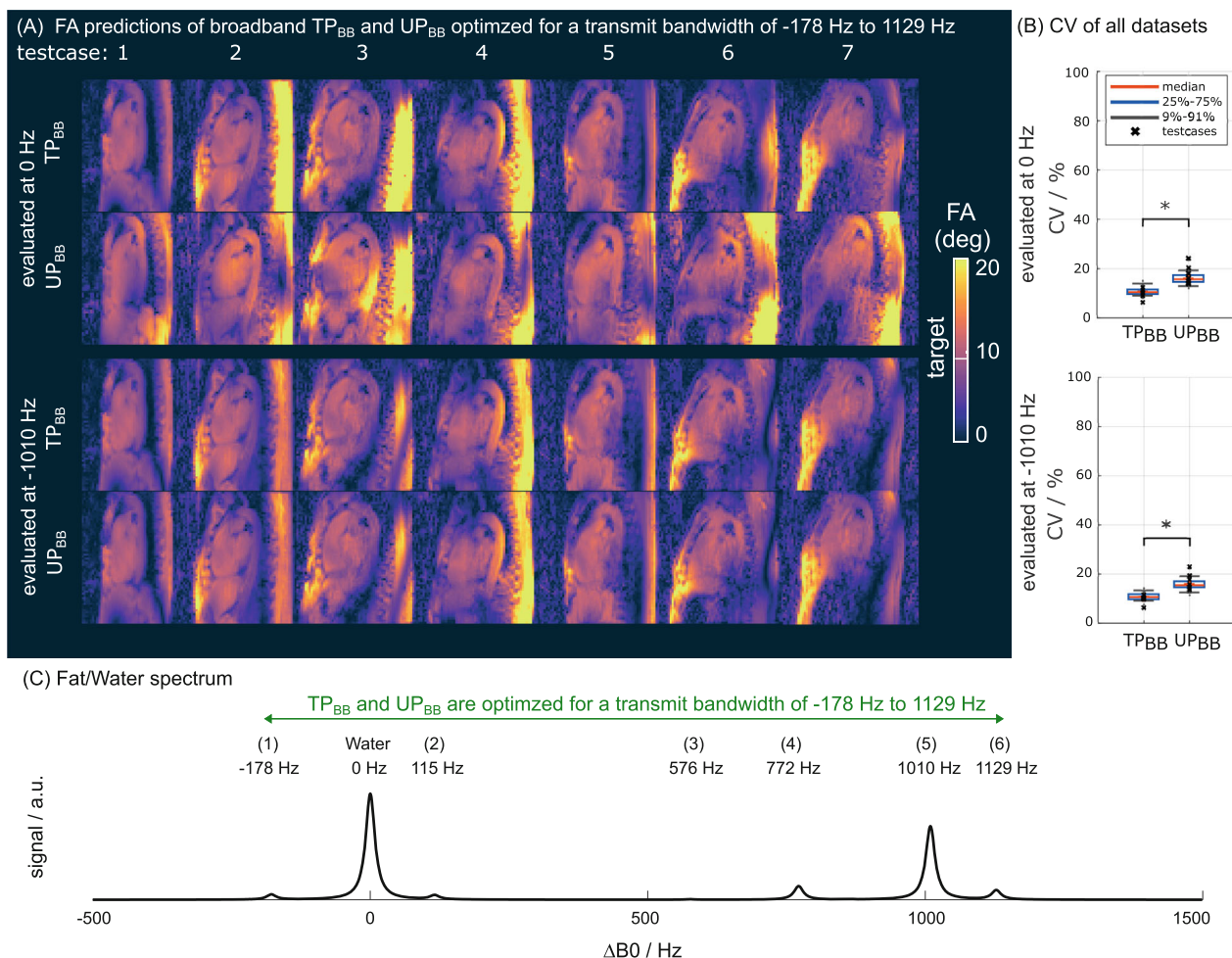


FIGURE 2 FA predictions of broadband tailored (TP_{BB}) and universal (UP_{BB}) pulses evaluated at 0 Hz (water) and 1010 Hz (fat). (A) Sagittal views of the same slices as in Figure 1, demonstrating FA homogeneity at both water and fat frequencies. (B) Quantitative assessment of predicted FA homogeneity across all target volumes (shown in Figure 1) assessed at 0 Hz and 1010 Hz revealing low CV values of below 23% for TP_{BB} and UP_{BB}. Statistically significant outcomes are denoted by a star (*), while non-statistically significant results are indicated as “NS”. (C) Model fat and water spectrum indicating which frequencies have been optimized in the pulse design. Peak numbering (1), (2), etc. is taken from Hamilton et al.⁴⁰

evaluated at 0 Hz and 1010 Hz (main fat peak at 7T). Figure 1A displays sagittal views of the 3D volume, highlighting the FA homogeneity at the water frequency but also the significant spatial variations and dropouts at the fat frequency. Figure 1B provides a quantitative assessment of FA homogeneity across the heart volumes of all datasets. Across the 29 datasets, the evaluation at 0 Hz yielded low CV values, with a mean of 6.4%/12.8% for TP_S/UP_S and 38%/49% at 1010 Hz. Figure 1C provides a schematic model fat and water spectrum (the signal amplitude is for illustrative purposes only and was not considered in the pulse design) indicating which frequencies were used in the optimization.⁴⁰

Figure 2 presents the FA predictions of broadband optimized TP_{BB}/UP_{BB} with a fixed pulse duration of 0.96 ms evaluated at 0 and 1010 Hz. Figure 2A displays sagittal views of the 3D volume, highlighting the FA homogeneity

at the water and fat frequency. Figure 2B provides a quantitative assessment of FA homogeneity across the entire target volumes of all datasets. The TP_{BB}/UP_{BB} evaluation at 0 Hz yielded low CV values, with a mean of 10%/15.4%. In contrast to the results shown in Figure 1, low CV values were also observed when evaluating the TP_{BB}/UP_{BB} at 1010 Hz, with a mean of 10.4%/15.3%. Figure 2C provides a model fat and water spectrum indicating which frequencies were used in the optimization. The spatial phase profile evaluated at 0 Hz and 1010 Hz after the application of TP_{BB} is shown in Figure S2.

Figure 3 illustrates the performance of various TP/UP optimized for different resonance frequencies ($f_S/f_D/f_{BB}$) with pulse durations ranging from 0.384 to 3.840 ms. Figure 3A displays a representative sagittal slice of testcase #2, showcasing the TP/UP evaluations with fixed pulse duration of 0.96 ms at three resonance frequencies (0, 576,

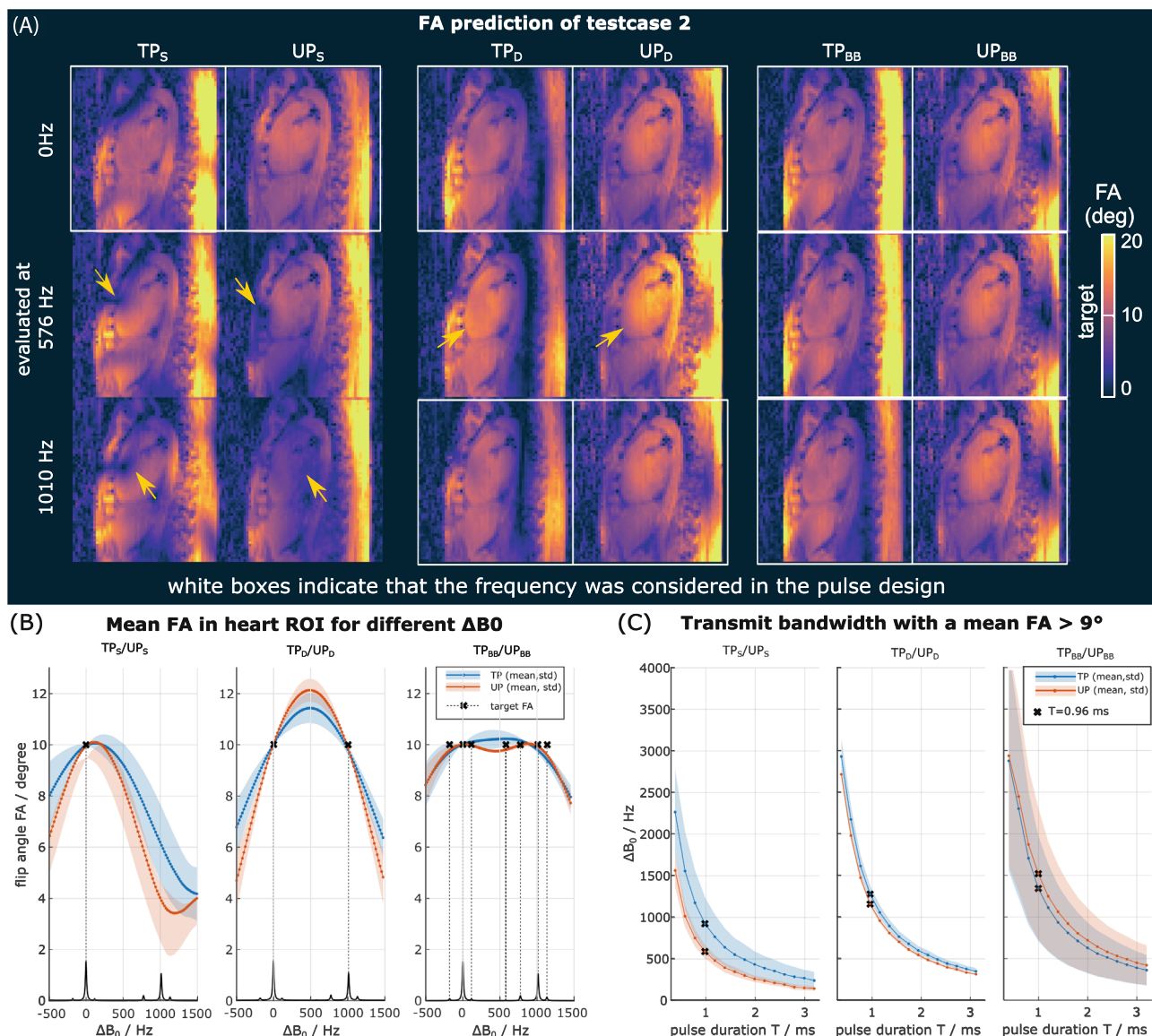


FIGURE 3 Performance analysis of tailored and universal pTx pulses (TP/UP) with different pulse durations optimized for specific frequencies (f_s , f_D and f_{BB}). (A) The sagittal slice of testcase #2 shows the evaluation of TP/UP pulses with fixed pulse duration of 0.96 ms at three frequencies (0, 576, and 1010 Hz). TP_S/UP_S and TP_D/UP_D exhibit inhomogeneous FA predictions for frequencies not included in the optimization. Broadband pulses demonstrate consistent FA predictions across all frequencies. (B) Mean FA and SD within the target volume for all five testcases, focusing on a ΔB_0 interval from -500 to 1500 Hz (small circles mark the evaluated frequency). Broadband pulses yield a FA distribution with minimal deviations within the 1307 Hz frequency range. (C) Transmit bandwidth where TP/UP pulses, with pulse durations (the entire kT-points train) ranging from 0.384 to 3.84 ms, achieve a mean FA exceeding 9° within the heart region. Broadband pulses demonstrate the broadest bandwidth, thus outperforming TP_S/UP_S regarding off-resonance variations.

and 1010 Hz). As expected, TP_S/UP_S and TP_D/UP_D achieve FA homogeneity only at those frequencies they were optimized for, while the broadband pulses result in consistent and homogeneous FA predictions across all frequencies. Figure S3 shows the evaluation for all seven frequencies, while S4 exhibits three orthogonal planes for two frequencies supporting the summarized findings in Figure 3A.

Figure 3B presents the mean and SD of the FA within the target volume for all seven testcases. The target FAs

for each pulse type are shown by black crosses. Notably, TP_D and UP_D shows an overshoot for ΔB_0 values between 0 Hz and 1010 Hz. In contrast, TP_{BB}/UP_{BB} yield low FA variations across all target FAs, with maximum absolute deviations of less than 0.5° .

Figure 3C depicts the computed transmit bandwidth where TP/UP, with pulse durations ranging from 0.384 to 3.840 ms, achieve a mean FA exceeding 9° . For example, at a pulse duration of 0.96 ms, the mean transmit bandwidth

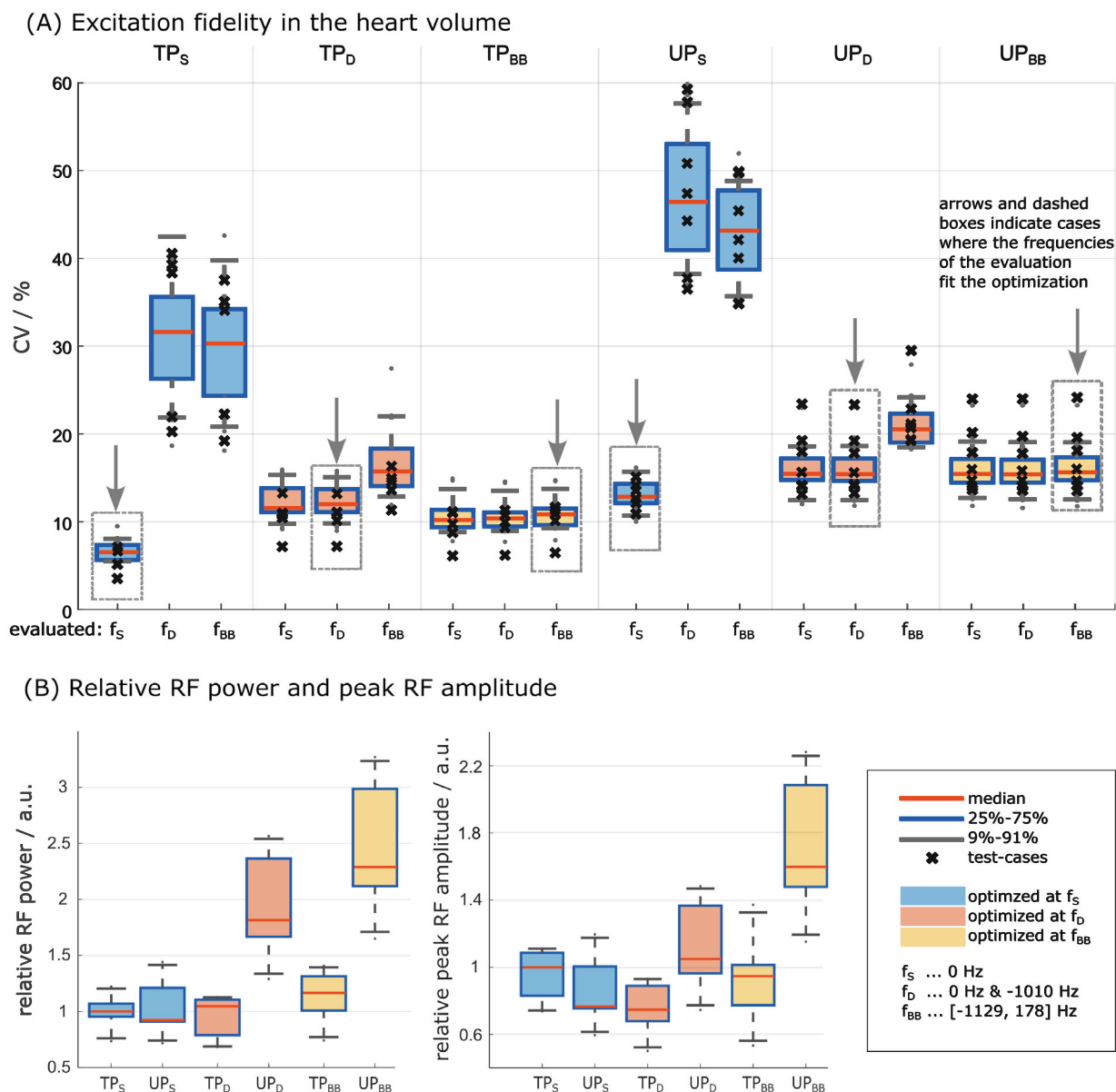


FIGURE 4 (A) Quantitative evaluation of FA predictions in target regions using TP and UP with a fixed pulse duration of $T = 0.96$ ms. Results across 27 volunteers demonstrate poor FA homogeneity for frequencies other than the optimized frequency. Similarly, UPs exhibit higher CV values but follow the same trend. Robustness across all frequencies is achieved with pulses optimized for all seven frequencies. These findings highlight the importance of broadband pulse optimization for consistent FA predictions across different frequencies. (B) Relative RF power and RF peak amplitude overview for different pulse types, revealing increased requirements for UP compared to TP. Statistically significant outcomes are denoted by a star (*), while non-statistically significant results are indicated as “NS”.

was 925 Hz for TP_s and 591 Hz for UP_s . In contrast, the TP_{BB}/UP_{BB} yielded a much higher transmit bandwidth of 1625/1768 Hz. Please note that TP_D/UP_D can exhibit superior performance in terms of transmit bandwidth. However, the FA homogeneity of TP_D/UP_D consistently fell short of that achieved by TP_{BB}/UP_{BB} (as depicted in Figure 3B).

Figure 4 presents the quantitative evaluation of FA predictions in the target regions of TP/UP with a fixed pulse duration of 0.96 ms. Arrows and dashed boxes indicate

cases where the frequencies of the evaluation match the optimization. In summary, robustness across all frequencies (f_{BB}) was only achieved with pulses optimized for all seven frequencies, resulting in mean CV values of 10.8% (TP_{BB}) and 15.6% (UP_{BB}). Consequently, TP_{BB}/UP_{BB} demonstrate favorable performance for $f_s/f_D/f_{BB}$, while TP_s/UP_s perform well only for f_s and exhibit increased CVs for f_D/f_{BB} . Figure 4B provides an overview of the relative RF power and peak RF amplitude requirements for the different TP/UP. The RF and gradient

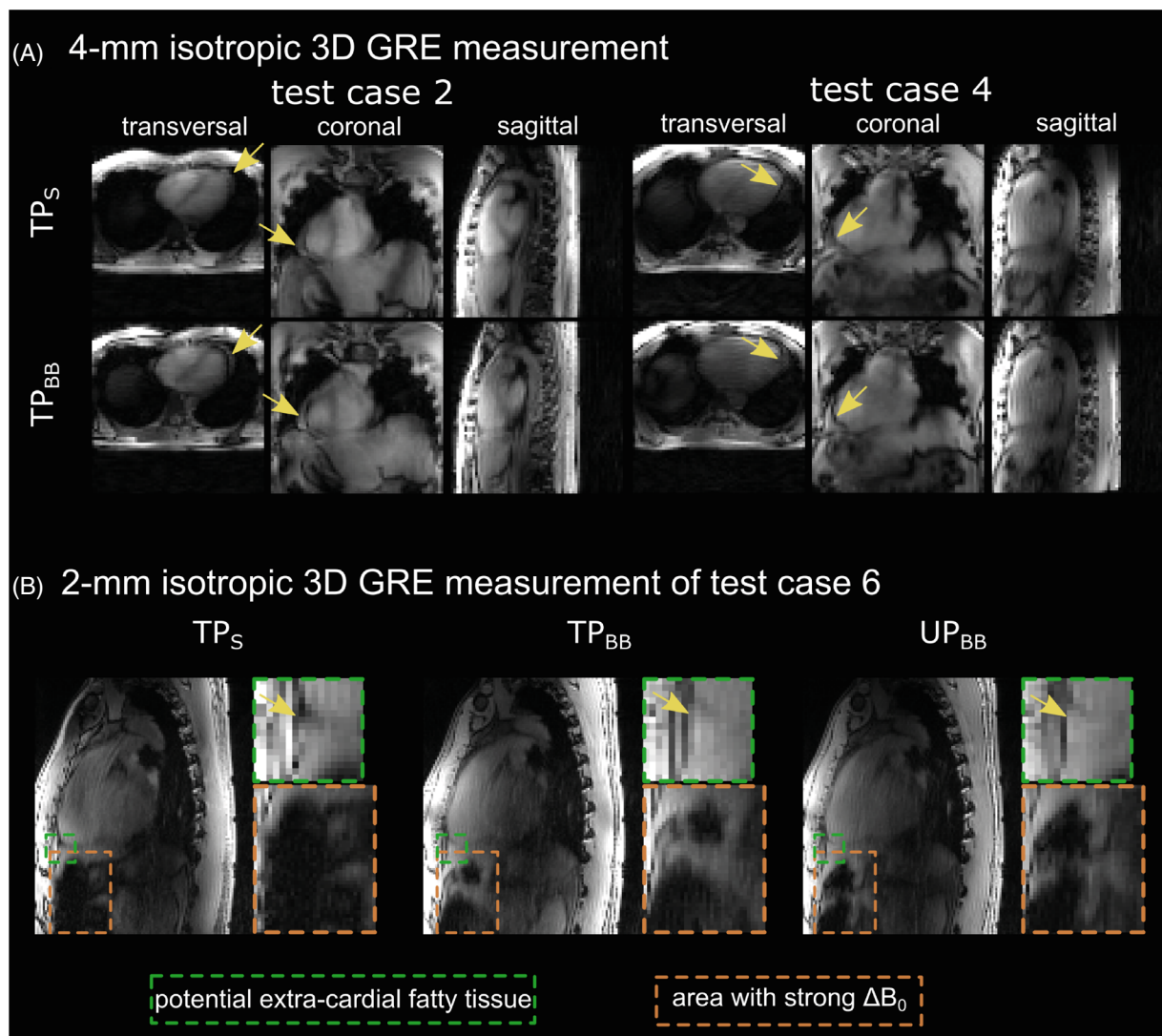


FIGURE 5 The 3D GRE images during free breathing, showcasing the improved signal homogeneity of the broadband TP_{bb} in areas with potentially fatty tissue and strong ΔB_0 variations (indicated by arrows and zoomed regions).

waveforms are shown in Figure S5. There is no significant disparity in RF power between the different TP, but UP consistently seems to require more power than TP. For instance, UP_{BB} requires approximately 2.3-times (2.0-times) more RF power compared to TP_S (TP_{BB}), respectively.

Figure 5 displays the 3D GRE images acquired during free breathing for three of the testcases utilizing TP_S , TP_{BB} , and UP_{BB} using the same peak RF voltage of 103.9 V. The lower RF efficiency of UP_{BB} contributes to reduced signal, but it also offers the advantage of being calibration-free, eliminating the need for approximately 15 min of adjustment time. Notably, compared to the single-frequency optimized TP_S , TP_{BB} and UP_{BB} exhibit a more homogeneous signal in volunteers with potentially fatty tissue surrounding the heart (indicated by arrows) and in areas with strong ΔB_0 variations.

4 | DISCUSSION

This study aimed to investigate the impact of resonance frequency differences on dynamic kT-points TP/UP and to research and evaluate a broadband TP/UP design more robust to chemical and ΔB_0 shifts in a cohort of 29 volunteers. The findings revealed that pulses designed solely based on the water frequency exhibited favorable performance only for water-like tissue, i.e., for 500 Hz around the water resonance frequency for 0.96 ms long pulses. Notably, the proposed broadband pulses effectively compensated for the differences in the FA homogeneity for resonance covering an extensive frequency range of 1307 Hz. While TP_{BB} requires similar RF power requirements to TP_S or TP_D , universal pulses required more RF power than TP. For instance, UP_{BB} requires approximately twice the RF power compared to TP_{BB} .

This study utilized a 3D B_1^+ -mapping method to acquire relative and channel-specific B_1^+ -maps, taking advantage of the RPE's short acquisition time and motion robustness. However, the resulting B_1^+ -maps are biased due to the assumption of equal magnitudes between transmit and receive channels.¹¹ Despite this limitation, the mapping method proved effective and has been successfully applied in various pTx applications at 7T, including calibration-free pTx via 3D UP for shallow breathing³¹ and respiration robust TP/UP of the human heart at 7T³⁰ and high-resolution fat/water imaging in the heart using static pTx.⁵

Tailored pTx in the human body can be challenging and time-consuming, particularly for the excitation of different respiration states or multiple resonance frequencies, due to increased computational demands and potential motion between B_1^+ -mapping and pTx data acquisition.^{8,12,30} The proposed broadband UP_{BB} provides a robust alternative to TP_{BB} for a 1307 Hz frequency range, including all six primary fat and the water peak, with acceptable FA homogeneity. On average, the broadband UP approach saves roughly 10–15 min of adjustment times for B_1^+ -acquisition (3:35 min), non-Cartesian reconstruction (1 min), manual ROI drawing (3 min), and pulse design and quality checks (up to 5 min).

In our previous works,^{12,41} relatively short pulse durations of 0.96 ms for dynamic pTx pulses effectively circumvented the impact of ΔB_0 off-resonance effects in the human heart of up to 350 Hz. This eliminates the need for additional time-consuming calibration processes, such as prolonged measurements of volunteer-specific ΔB_0 maps. However, covering the 1307 Hz frequency range required for simultaneous fat and water excitation proved impractical due to FA limitations, necessitating the research and development of the proposed broadband dynamic pTx pulse design.

A potential extension of this work would be to use GRAPE optimization instead of kT-points and focusing the ΔB_0 robustness target region specifically to human heart, as demonstrated in broadband GRAPE UPs for the human brain.³⁷ This could further reduce RF pulse duration, energy requirements, and/or improve homogeneity.

An unexpected yet consistent finding emerged across all testcases. The results of the two-frequency pulses exhibited an overshoot in FA predictions. While this trend was consistently observed in all testcases, drawing a broad conclusion regarding this effect would necessitate a more comprehensive range of testcases, exceeding the scope of this study.

This work has two major limitations. First, the absence of fat-water separated in vivo images limited our assessment of the observed excitation performance of broadband pulses. Second, the lack of absolute B_1^+ information in

the experimental scans restricted our approach to penalize the integrated relative RF power instead of the integrated actual RF power or the RF peak voltage. While the performed experiments primarily aimed at qualitatively validating relative B_1^+ predictions, absolute B_1^+ measurements are crucial for accurate FA quantification or designing large FA pulses. Therefore, it is essential to acknowledge that exact FA values remain unknown despite our understanding of the spatial B_1^+ patterns that can be scaled in the small tip angle regime. Future analyses will thus focus on integrating kT-point pulses into time-resolved 3D sequences, with specific attention given to techniques to achieve high-quality cardiac images at 7T.⁵

5 | CONCLUSIONS

This study presents two novel advancements in tailored and universal pulse design: simultaneous fat/water excitation for future fat/water imaging (e.g., Dixon) and broadband pulses robust to ΔB_0 inhomogeneities without requiring measured ΔB_0 information.

ACKNOWLEDGMENTS


We gratefully acknowledge funding from the German Research Foundation SCHM 2677/2-1 SCHM 2677/4-1 and GRK2260, BIOQIC. Open Access funding enabled and organized by Projekt DEAL.

DATA AVAILABILITY STATEMENT

The source code, the used parameters, and the 3D relative B_1^+ datasets can be found at: https://github.com/chaigner/FRobUP_body.

ORCID

Christoph Stefan Aigner  <https://orcid.org/0000-0003-3618-9610>

Sebastian Dietrich-Conzelmann  <https://orcid.org/0000-0002-1610-909X>

Max Lutz  <https://orcid.org/0009-0001-1956-3757>

Felix Krüger  <https://orcid.org/0000-0001-9453-8992>

Sebastian Schmitter  <https://orcid.org/0000-0003-4410-6790>

REFERENCES

- Ladd ME, Bachert P, Meyerspeer M, et al. Pros and cons of ultra-high-field MRI/MRS for human application. *Prog Nucl Magn Reson Spectrosc*. 2018;109:1-50. doi:10.1016/j.pnmrs.2018.06.001
- Williams SN, McElhinney P, Gunamony S. Ultra-high field MRI: parallel-transmit arrays and RF pulse design. *Phys Med Biol*. 2023;68:02TR02. doi:10.1088/1361-6560/aca4b7

3. Niendorf T, Paul K, Oezerdem C, et al. W(h)ither human cardiac and body magnetic resonance at ultrahigh fields? Technical advances, practical considerations, applications, and clinical opportunities: advances in ultrahigh field cardiac and body magnetic resonance. *NMR Biomed.* 2016;29:1173-1197. doi:10.1002/nbm.3268
4. Kellman P, Hernando D, Arai AE. Myocardial fat imaging. *Curr Cardiovasc Imaging Rep.* 2010;3:83-91. doi:10.1007/s12410-010-9012-1
5. Dietrich S, Aigner CS, Mayer J, et al. Motion-compensated fat-water imaging for 3D cardiac MRI at ultra-high fields. *Magn Reson Med.* 2022;87:2621-2636. doi:10.1002/mrm.29144
6. Kraff O, Quick HH. Radiofrequency coils for 7 tesla MRI. *Top Magn Reson Imaging.* 2019;28:145-158. doi:10.1097/RMR.0000000000000206
7. Yang QX, Mao W, Wang J, et al. Manipulation of image intensity distribution at 7.0 T: passive RF shimming and focusing with dielectric materials. *J Magn Reson Imaging.* 2006;24:197-202. doi:10.1002/jmri.20603
8. Padormo F, Beqiri A, Hajnal JV, Malik SJ. Parallel transmission for ultrahigh-field imaging: parallel transmission for ultrahigh-field imaging. *NMR Biomed.* 2016;29:1145-1161. doi:10.1002/nbm.3313
9. Schmitter S, DelaBarre L, Wu X, et al. Cardiac imaging at 7 tesla: single- and two-spoke radiofrequency pulse design with 16-channel parallel excitation: cardiac imaging at 7T. *Magn Reson Med.* 2013;70:1210-1219. doi:10.1002/mrm.24935
10. Schmitter S, Schnell S, Uğurbil K, Markl M, Van de Moortele PF. Towards high-resolution 4D flow MRI in the human aorta using kt-GRAPPA and B1+ shimming at 7T: aortic 4D flow MRI at 7T with kt-GRAPPA. *J Magn Reson Imaging.* 2016;44:486-499. doi:10.1002/jmri.25164
11. Dietrich S, Aigner CS, Kolbitsch C, et al. 3D free-breathing multichannel absolute mapping in the human body at 7T. *Magn Reson Med.* 2021;85:2552-2567. doi:10.1002/mrm.28602
12. Aigner CS, Dietrich S, Schmitter S. Three-dimensional static and dynamic parallel transmission of the human heart at 7 T. *NMR Biomed.* 2021;34:e4450. doi:10.1002/nbm.4450
13. Runderkamp BA, Roos T, van der Zwaag W, Strijkers GJ, Caan MWA, Nederveen AJ. Whole-liver flip-angle shimming at 7T using parallel-transmit kT-point pulses and Fourier phase-encoded DREAM B1+ mapping. *Magn Reson Med.* 2024;91:75-90. doi:10.1002/mrm.29819
14. Grimm J, Aigner CS, Dietrich S, et al. In-vivo 3D liver imaging at 7T using kT-point pTx pulses and a 32-Tx-channel whole-body RF antenna array. *Proceedings of the 21th Annual Meeting of ISMRM.* 1419;2023.
15. Katscher U, Börner P, Leussler C, Van Den Brink JS. Transmit SENSE: Transmit SENSE. *Magn Reson Med.* 2003;49:144-150. doi:10.1002/mrm.10353
16. Zhu Y. Parallel excitation with an array of transmit coils. *Magn Reson Med.* 2004;51:775-784. doi:10.1002/mrm.20011
17. Setsompop K, Alagappan V, Gagoski B, et al. Slice-selective RF pulses for in vivo B1+ inhomogeneity mitigation at 7 tesla using parallel RF excitation with a 16-element coil: in vivo slice-selective parallel excitation. *Magn Reson Med.* 2008;60:1422-1432. doi:10.1002/mrm.21739
18. Orzada S, Maderwald S, Poser BA, Bitz AK, Quick HH, Ladd ME. RF excitation using time interleaved acquisition of modes (TIAMO) to address B₁ inhomogeneity in high-field MRI. *Magn Reson Med.* 2010;64:327-333. doi:10.1002/mrm.22527
19. Cloos MA, Boulant N, Luong M, et al. kT-points: short three-dimensional tailored RF pulses for flip-angle homogenization over an extended volume. *Magn Reson Med.* 2012;67:72-80. doi:10.1002/mrm.22978
20. Malik SJ, Keihaninejad S, Hammers A, Hajnal JV. Tailored excitation in 3D with spiral nonselective (SPINS) RF pulses: spiral nonselective (SPINS) RF pulses. *Magn Reson Med.* 2012;67:1303-1315. doi:10.1002/mrm.23118
21. Grissom WA, Khalighi MM, Sacolick LI, Rutt BK, Vogel MW. Small-tip-angle spokes pulse design using interleaved greedy and local optimization methods: interleaved greedy and local spokes pulse design. *Magn Reson Med.* 2012;68:1553-1562. doi:10.1002/mrm.24165
22. Prieto C, Uribe S, Razavi R, Atkinson D, Schaeffter T. 3D undersampled golden-radial phase encoding for DCE-MRA using inherently regularized iterative SENSE. *Magn Reson Med.* 2010;64:514-526. doi:10.1002/mrm.22446
23. Buerger C, Clough RE, King AP, Schaeffter T, Prieto C. Nonrigid motion modeling of the liver from 3-D Undersampled self-gated Golden-radial phase encoded MRI. *IEEE Trans Med Imaging.* 2012;31:805-815. doi:10.1109/TMI.2011.2181997
24. Waxmann P, Mekle R, Schubert F, et al. A new sequence for shaped voxel spectroscopy in the human brain using 2D spatially selective excitation and parallel transmission: shaped voxel excitation MRS using a transmit array. *NMR Biomed.* 2016;29:1028-1037. doi:10.1002/nbm.3558
25. Bosch D, Bause J, Geldschläger O, Scheffler K. Optimized ultrahigh field parallel transmission workflow using rapid presaturated TurboFLASH transmit field mapping with a three-dimensional centric single-shot readout. *Magn Reson Med.* 2023;89:322-330. doi:10.1002/mrm.29459
26. Cao Z, Yan X, Grissom WA. Array-compressed parallel transmit pulse design: Array-compressed parallel transmit pulse design. *Magn Reson Med.* 2016;76:1158-1169. doi:10.1002/mrm.26020
27. Gras V, Vignaud A, Amadon A, Bihan D, Boulant N. Universal pulses: a new concept for calibration-free parallel transmission. *Magn Reson Med.* 2017;77:635-643. doi:10.1002/mrm.26148
28. Herrler J, Liebig P, Gumbrecht R, et al. Fast online-customized (FOCUS) parallel transmission pulses: a combination of universal pulses and individual optimization. *Magn Reson Med.* 2021;85:3140-3153. doi:10.1002/mrm.28643
29. Le Ster C, Mauconduit F, Massire A, Boulant N, Gras V. Standardized universal pulse: a fast RF calibration approach to improve flip angle accuracy in parallel transmission. *Magn Reson Med.* 2022;87:2839-2850. doi:10.1002/mrm.29180
30. Aigner CS, Dietrich S, Schmitter S. Respiration induced B1+ changes and their impact on universal and tailored 3D kT-point parallel transmission pulses for 7T cardiac imaging. *Magn Reson Med.* 2022;87:2862-2871. doi:10.1002/mrm.29183
31. Aigner CS, Dietrich S, Schaeffter T, Schmitter S. Calibration-free pTx of the human heart at 7T via 3D universal pulses. *Magn Reson Med.* 2022;87:70-84. doi:10.1002/mrm.28952
32. Dixon WT. Simple proton spectroscopic imaging. *Radiology.* 1984;153:189-194. doi:10.1148/radiology.153.1.6089263
33. Glover GH. Multipoint dixon technique for water and fat proton and susceptibility imaging. *J Magn Reson Imaging.* 1991;1:521-530. doi:10.1002/jmri.1880010504

34. Reeder SB, Pineda AR, Wen Z, et al. Iterative decomposition of water and fat with echo asymmetry and least-squares estimation (IDEAL): application with fast spin-echo imaging. *Magn Reson Med*. 2005;54:636-644. doi:10.1002/mrm.20624
35. Setsompop K, Alagappan V, Gagoski BA, et al. Broad-band slab selection with B mitigation at 7T via parallel spectral-spatial excitation. *Magn Reson Med*. 2009;61:493-500. doi:10.1002/mrm.21834
36. Khaneja N, Reiss T, Kehlet C, Schulte-Herbrüggen T, Glaser SJ. Optimal control of coupled spin dynamics: design of NMR pulse sequences by gradient ascent algorithms. *J Magn Reson*. 2005;172:296-305. doi:10.1016/j.jmr.2004.11.004
37. Van Damme L, Mauconduit F, Chambrion T, Boulant N, Gras V. Universal nonselective excitation and refocusing pulses with improved robustness to off-resonance for magnetic resonance imaging at 7 tesla with parallel transmission. *Magn Reson Med*. 2021;85:678-693. doi:10.1002/mrm.28441
38. Krueger F, Aigner CS, Hammernik K, et al. RAPID estimation of 2D relative B1+-maps from localizers in the human heart at 7T using deep learning. *Magn Reson Med*. 2023;89:1002-1015. doi:10.1002/mrm.29510
39. Smith D, Berglund J, Kullberg J, Ahlström H, Avison M, Welch E. Optimization of fat-water separation algorithm selection and options using image-based metrics with validation by ISMRM fat-water challenge datasets. *Proceedings of the 21th Annual Meeting of ISMRM*. 2413;2013.
40. Hamilton G, Yokoo T, Bydder M, et al. *In vivo* characterization of the liver fat ¹H MR spectrum. *NMR Biomed*. 2011;24:784-790. doi:10.1002/nbm.1622
41. Hock M, Terekhov M, Stefanescu MR, et al. B₀ shimming of the human heart at 7T. *Magn Reson Med*. 2021;85:182-196. doi:10.1002/mrm.28423

SUPPORTING INFORMATION

Additional supporting information may be found in the online version of the article at the publisher's website.

FIGURE S1: Evaluation of tailored pulses in phantom experiments. (A) GRE images of a dual-phantom experiment (doped water and rapeseed oil) to assess the excitation fidelity of various tailored pulses. The broadband TP effectively excites both water and fat, while the single-frequency pulse (water only TP) exhibits reduced excitation in the oil phantom. (B) Phantom study using a PVP phantom and TP_S, TP_D and TP_{BB} at varying resonance

frequencies reveal the impact of off-resonance on excitation. TP_S experiences severe artifacts above ± 250 Hz, while TP_D and TP_{BB} demonstrate a wider transmit bandwidth and improved resistance to off-resonance effects. These results are consistent with in-vivo observations, showing a slight overshoot for TP_D and uniform signal for TP_{BB} within the optimized frequency range.

FIGURE S2: The phase of a non-selective block pulse and tailored broadband pulses (TP_{BB}) across the target frequency range (0 and 1010 Hz). The non-selective rectangular block pulse results in a similar spatial phase distribution that can be corrected by a global phase shift (because of the different resonance frequencies of fat and water at 7 T).

FIGURE S3: 3D flip-angle (FA) predictions for one sagittal slice in one out of five testcases evaluated at seven frequencies for different TP/UP. TP_S/UP_S optimized for one frequency are robust for approximately ± 200 Hz because of the relatively short pulse duration of 0.96 ms. However, more considerable frequency variations such as 1010 or 1129 Hz result in significant dropouts that can be successfully compensated by considering more frequencies in the pulse design. The other four testcases show the same trend.

FIGURE S4: 3D flip-angle (FA) predictions in one out of five testcases for different TP/UP evaluated at two frequencies (0 and 1010 Hz). This qualitative comparison demonstrates the need to consider multiple frequencies if water and fat should be acquired simultaneously. Although not shown, the other four testcases show the same trend.

FIGURE S5: Pulse diagram showing the RF pulses (magnitude and phase) and 3D gradient blips of the different tailored and universal pulses (TP/UP), optimized for a different combination of resonance frequency peaks.

How to cite this article: Aigner CS, Dietrich-Conzelmann S, Lutz M, Krüger F, Schmitter S. Tailored and universal parallel transmit broadband pulses for homogeneous 3D excitation of the human heart at 7T. *Magn Reson Med*. 2024;92:730-740. doi: 10.1002/mrm.30072